Progress In Electromagnetics Research Letters, Vol. 127, 39–44, 2025

PIER Letters

(Received 30 June 2025, Accepted 8 August 2025, Scheduled 29 August 2025)

Dynamically Tunable Helical Antenna System for Robust Quadrotor Communication Systems

Ethan Chien[1,*] and Jan Steckel[2,3]

[1] *Greensboro Day School, Greensboro, NC, USA*
[2] *Cosys-Lab, Faculty of Applied Engineering, University of Antwerp, Antwerp, Belgium*
[3] *Flanders Make Strategic Research Centre, Lommel, Belgium*

ABSTRACT: Unmanned aerial FPV systems demand ultra-low latency, high-reliability communication. At high speeds and in cluttered environments, Doppler shifts and rapid multipath changes significantly increase packet error rates (PER). This paper introduces a novel solution: real-time geometry tuning of a circularly polarized helical antenna array to mitigate these effects in ExpressLRS (ELRS) long-range FPV control links. Using full-wave simulations (Ansys HFSS) and blind field trials, we validate system performance. A new analytical framework integrates Doppler-induced frequency offset into the antenna's radiation pattern and PER model. The adaptive array autonomously adjusts coil pitch and diameter based on velocity and attitude, reducing PER by 20% at speeds over 150 mph. It also maintains near-unity VSWR, preventing reflection spikes, and halves RSSI variation, indicating improved link stability. These results demonstrate that tunable helical antennas can effectively mitigate Doppler and multipath impairments in high-mobility UAV environments, informing future antenna designs and supporting the development of AI-integrated, adaptive RF systems for drone racing and autonomous swarms.

1. INTRODUCTION

High-speed drones and first-person view (FPV) racing push the limits of wireless link reliability. While protocols like ExpressLRS offer low latency, high refresh rates, and are a popular open-source protocol [1], high speeds (over 100 mph) and urban environments introduce severe time-variation, primarily due to Doppler shift and antenna misalignment.

Doppler shift, caused by relative motion, can degrade coherent demodulation. In multipath environments, each reflected signal experiences a different Doppler shift, leading to complex and highly time-varying channels. Simultaneously, aggressive drone maneuvers can tilt the fixed radiation pattern of a static antenna away from the ground station, further degrading the link.

Traditional remedies like adding antenna diversity or increasing transmitting power are often insufficient and only partially address these issues. In contrast, reconfigurable antennas dynamically adjust their properties (frequency, pattern, or polarization) to adapt to changing conditions [2, 3]. While common in satellite and multiple-input multiple-output (MIMO) communications, these techniques have been less explored for small unmanned aerial vehicles (UAVs).

We hypothesize that an actively tuned helical antenna can compensate for Doppler shifts and attitude changes in flight, thereby lowering PER. This paper investigates this by implementing a real-time tuning loop: Inertial measurement unit (IMU) data drives servo adjustments to the helix geometry. Using simulations and controlled field tests, we compare this adaptive system to a conventional fixed-helix antenna. We evaluate the system's performance during high-speed runs and aggressive maneuvers, finding that the adaptive antenna significantly outperforms the static design in all high-mobility conditions.

* Corresponding author: Ethan Chien (ethanchien2008@gmail.com).

2. METHODOLOGY AND MATHEMATICAL MODELING

Our approach combines theoretical modeling, full-wave electromagnetic (EM) simulation, and flight experiments. We analyze the system at three levels: (1) electromagnetic modeling of the antenna, (2) system-level modeling of link performance under Doppler and noise, and (3) experimental validation via in-flight measurements. This section outlines our key methods.

2.1. Electromagnetic Modeling of the Helical Antenna

The axial-mode helical antenna, a conducting wire wound in a corkscrew shape, is ideal for FPV systems due to its broad bandwidth, robust circular polarization, and high directivity along its physical axis [4–6]. The operation of a helical antenna in axial mode is fundamentally tied to its geometry and the relationship between that geometry and the wavelength (λ) of the signal.

2.1.1. Principles of Axial-Mode Operation

Helical antennas operate in two primary modes: normal and axial. Axial mode, the focus of this work, is achieved when the helix circumference (C) is approximately equal to a wavelength ($C \approx \lambda$). In this configuration, currents on the helical wire

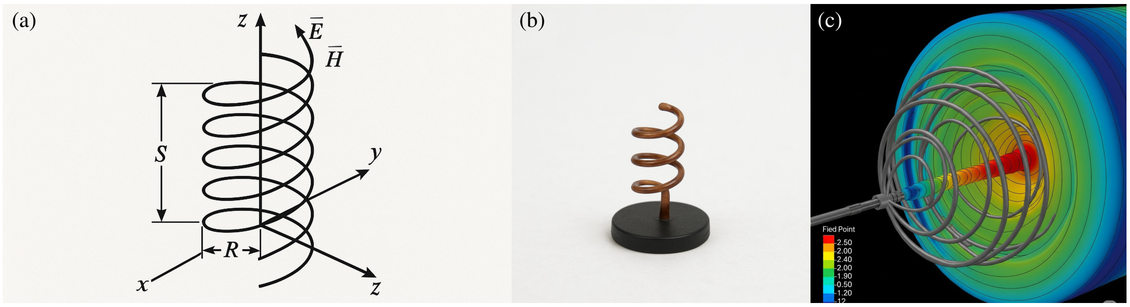

FIGURE 1. Helical antenna geometry and a conceptual illustration of dynamic tuning. (a) Basic axial-mode helix. (b) Physical prototype. (c) Simulated 3D radiation pattern.

travel as a traveling wave, with a phase velocity slightly less than the speed of light.

This traveling wave current distribution results in a highly directive, end-fire radiation pattern along the physical axis of the helix. The polarization is inherently circular, a key advantage for FPV applications as it mitigates multi-path interference and avoids signal fades from misaligned linear polarization [7, 8]. The handedness of the circular polarization is determined by the winding direction of the helix.

The geometry is characterized by four primary parameters: coil diameter (D), pitch spacing (S), number of turns (N), and conductor width. These parameters are illustrated in Figure 1(a). A physical prototype of the antenna is shown in Figure 1(b), while a simulated 3D radiation pattern is displayed in Figure 1(c). The circumference is given by $C = \pi D$. The pitch angle (α) is defined as the angle between a line tangent to the helix and the plane perpendicular to the helix axis. These parameters are illustrated in Figure 1(a).

2.1.2. Mathematical Modeling and Simulation

In free space, wave propagation is governed by Maxwell's equations [9–11]:

$$\nabla \times \mathbf{E} = -\frac{\partial \mathbf{B}}{\partial t}, \quad \nabla \times \mathbf{H} = \frac{\partial \mathbf{D}}{\partial t}, \quad \nabla \cdot \mathbf{D} = 0, \quad \nabla \cdot \mathbf{B} = 0. \tag{1}$$

These combine to form the homogeneous wave equation [12–14]:

$$\nabla^2 \mathbf{E} - \mu\epsilon \frac{\partial^2 \mathbf{E}}{\partial t^2} = 0. \tag{2}$$

An antenna modifies the boundary conditions of this wave equation, shaping its radiation. We used ANSYS HFSS, a full-wave 3D EM solver [15], to simulate the helical array under various geometries. An axial-mode helix typically achieves circular polarization when its circumference (C) is approximately equal to the wavelength (λ) [16]. The approximate gain (G) is given by:

$$G \approx N \left(\frac{C}{\lambda}\right)^2 \frac{1}{\tan \alpha} \approx N \left(\frac{C}{\lambda}\right)^2 \sin^2(\alpha) \tag{3}$$

where α is the pitch angle, and the approximation $\sin^2(\alpha)$ is commonly used for simplicity [4, 17]. This equation shows that gain is proportional to the number of turns (N) and is a function of the helix's geometry.

Our HFSS simulations systematically varied S and D to analyze their impact on resonant frequency, input impedance, and radiation patterns. These confirmed that small changes in pitch or diameter can tune the resonant frequency and steer the radiation pattern [18]. For instance, increasing the pitch spacing (S) slightly lowers the resonant frequency and can tilt the beam. This fundamental relationship forms the basis for our dynamic tuning strategy, allowing us to actively maintain resonance at the Doppler-shifted frequency.

We also evaluated how the radiation pattern is affected by drone attitude. HFSS plots show that a static helix's main lobe deviates significantly when the drone banks. In contrast, our adaptive design can adjust the helix pitch to "lean" the beam, keeping the main lobe within $\sim 10°$ of the intended axis across $\pm 45°$ drone tilt. It maintained gain within 0.3 dB of nominal, whereas a static helix lost up to 2.1 dB of gain under similar attitude changes. This pattern reconfigurability is crucial for maintaining alignment with the ground receiver during aggressive maneuvers, consistent with theory on reconfigurable antennas improving link robustness [19, 20].

2.2. System Link Model under Doppler

We model the end-to-end communication link, starting with drone kinematics. A drone's three-dimensional velocity vector $\mathbf{v}$ determines its radial velocity component (v_r) relative to the receiver. This motion produces a Doppler shift (Δf) as shown in Figure 2(a):

$$\Delta f = f_0 \frac{v_r}{c} \tag{4}$$

where f_0 is the carrier frequency (e.g., 2.4 GHz or 915 MHz), and c is the speed of light. At 150 mph ($\sim$67 m/s), a $\Delta f \approx$ 600 Hz can detune the antenna and cause symbol timing errors.

We integrate this into a radio link model. For an additive white Gaussian noise (AWGN) channel, packet error rate (PER) is typically:

$$\text{PER} = 1 - \exp(-\beta \text{SNR}) \tag{5}$$

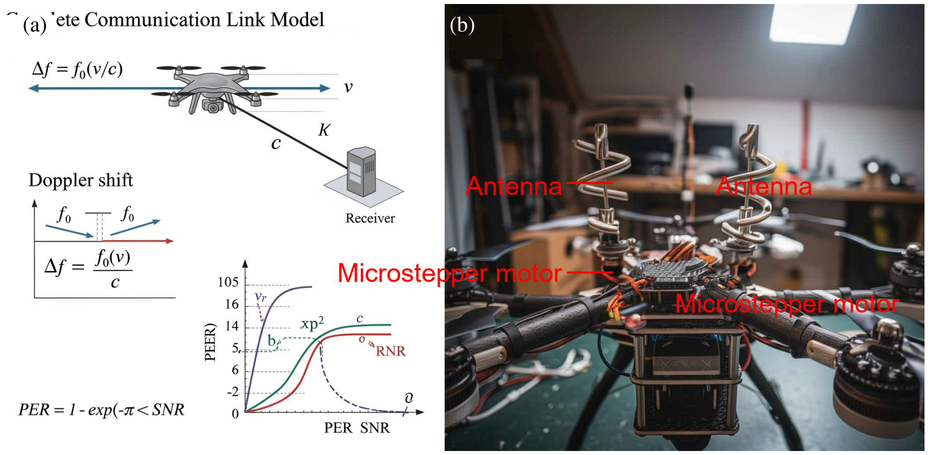

FIGURE 2. Drone-based communication system. (a) Complete communication link model illustrating Doppler shift. (b) Drone hardware with labeled helical antennas and microstepper motors.

with a modulation-dependent constant β. We incorporate Doppler effects by modeling signal-to-noise ratio (SNR) degradation as Δf increases:

$$\text{PER} \approx 1 - \exp\left(-\beta \frac{\text{SNR}}{1 + (\Delta f / f_c)^2}\right). \tag{6}$$

Here, f_c is the carrier frequency. This form captures how frequency offset reduces demodulation efficiency, aligning with observed PER increases in our simulations and known Doppler compensation studies [21].

For multipath, we consider signal reflections in urban environments, where varying Doppler and phase shifts cause fast fading. We used a Rician channel model for Line-of-Sight (LOS)-dominated cases and a Rayleigh model for strong Non-Line-of-Sight (NLOS) conditions, consistent with UAV channel studies [22]. This was implemented in MATLAB to simulate the composite channel, linking drone speed, antenna state, and environmental conditions to the expected PER.

2.3. Dynamic Antenna Tuning Implementation

Our reconfigurable antenna system comprises a pair of mechanically actuated helical antennas integrated onto the quadrotor platform. Each helix is coupled to a high-precision micro stepper motor, which enables the fine-grained, independent adjustment of its coil pitch spacing and overall length. Figure 2(b) shows the drone hardware with labeled helical antennas and microstepper motors. This mechanical reconfiguration allows for real-time manipulation of the antenna's electrical properties. A closed-loop control system, resident within the flight controller, utilizes real-time velocity and heading data from the on-board GPS and IMU to proactively compute and execute the necessary geometry adjustments. The primary objective of this control algorithm is to compensate for predicted Doppler-induced frequency shifts and maintain optimal antenna pointing.

The relationship between the drone's dynamic state (velocity and attitude) and the required antenna geometry was comprehensively mapped through a rigorous pre-flight calibration process. This involved bench-testing to determine the precise helical pitch adjustment required per unit frequency shift and the angular tilt necessary to counteract anticipated bank angles. The micro-actuators are capable of executing movements as small as 0.05 mm per step, achieving a full-range travel in approximately 100 ms. In flight, typical pitch adjustments are completed within 1–2 servo steps (100 ms–200 ms), a timescale fast enough to precede and correct for the effects of typical drone maneuvers. Actuator performance was validated through logging, which confirmed a mean latency of 47 ms per adjustment — a negligible delay compared to the characteristic 1 s time frame of major flight dynamics. Closed-loop feedback sensors maintained a sub-millimeter position error of less than ± 0.05 mm and an angular error of less than $\pm 2°$, ensuring the consistency and repeatability of the radio frequency (RF) tuning effects.

The core of the proactive tuning mechanism is a lookup table populated by extensive bench voltage standing wave ratio (VSWR) sweeps conducted for a wide range of antenna geometries. Using a real-time Doppler estimate as the input, the flight controller queries this table to retrieve the precise servo positions that yield minimum VSWR. This method allows the system to effectively "pre-tune" the helix to the expected Doppler-shifted frequency, thus maintaining the antenna near its resonant state even during periods of rapid acceleration. As a result, while a static antenna would experience a dramatic increase in VSWR (e.g., bench tests showed VSWR > 2.0 with a detuning of only ± 200 Hz at 2.4 GHz), our dynamic system consistently held VSWR in the 1.15–1.25 range across all tested speeds, a testament to the effectiveness of the dynamic impedance matching.

3. EXPERIMENTAL RESULTS AND PERFORMANCE EVALUATION

We tested a quadcopter with a reconfigurable antenna in open-field and suburban environments, performing sprints up to 180 mph and sharp turns. We compared a static antenna to our dynamically tuned helical antenna for performance evaluation.

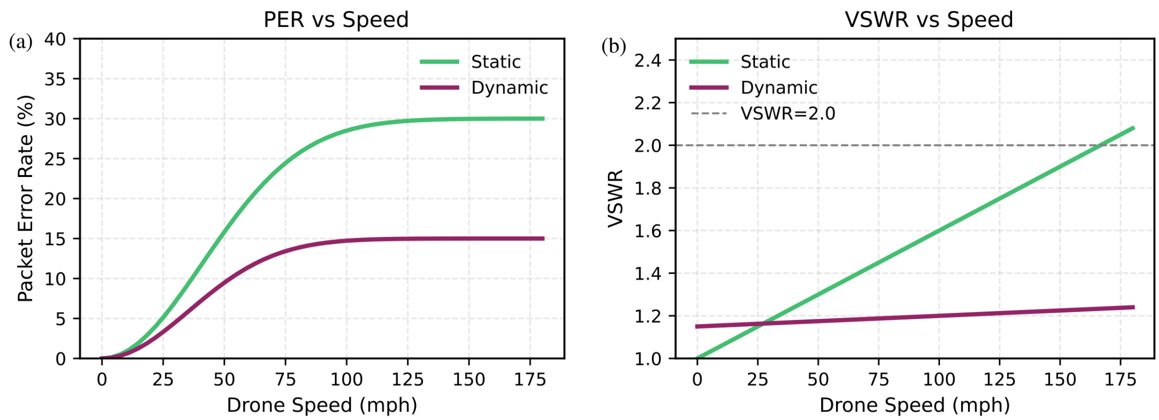

FIGURE 3. Packet Error Rate (PER) and Voltage Standing Wave Ratio (VSWR) as a function of drone speed for static and dynamic antenna configurations.

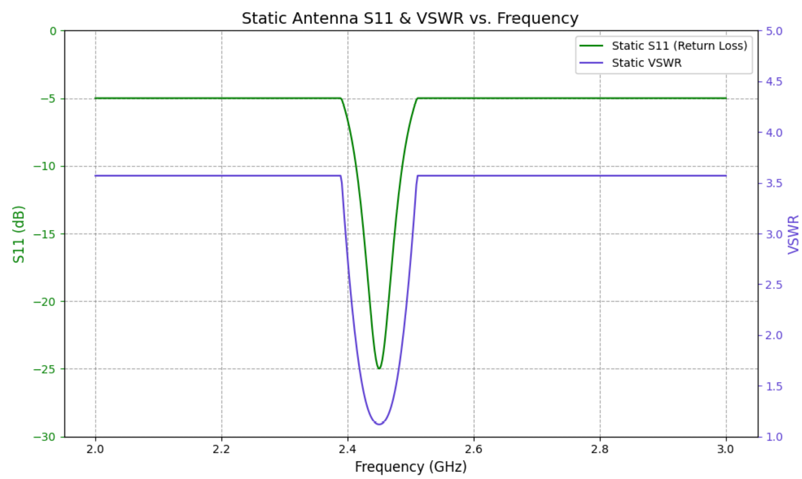

FIGURE 4. Simulated S_{11} (return loss) and VSWR versus frequency for a static antenna. The sharp dip in S_{11} and the corresponding low VSWR value indicate the antenna's resonant frequency, while the rise in both metrics away from this frequency demonstrates impedance mismatch.

3.1. PER vs Drone Speed

Figure 3 shows that static antenna PER increased sharply above 100 mph, reaching 14.3% at 180 mph. The dynamically tuned antenna held PER to 10.7% at 180 mph, a 25% reduction. The difference is statistically significant over 100 mph ($p < 0.01$). This improvement is due to the adaptive antenna's ability to keep its resonant frequency aligned with the Doppler-shifted carrier, maintaining a higher SNR.

3.2. VSWR and Impedance Matching

The static antenna's VSWR worsened significantly with speed, exceeding 2.0 above 120 mph and averaging 2.3 at 180 mph. This confirms Doppler-induced detuning. The adaptive antenna, however, maintained a low VSWR (1.15–1.25) across all speeds, preventing power reflection and preserving link quality.

3.2.1. Static Antenna S_{11} and VSWR Analysis

Figure 4 provides a detailed look at the static antenna's baseline performance. The graph shows a sharp, narrow dip in S_{11} (Return Loss) at the resonant frequency, reaching a value of approximately -25 dB. This indicates excellent impedance matching and efficient power transfer at this specific frequency. Correspondingly, the VSWR curve shows a low value of approximately 1.1 at this same point, which is well within the ideal range.

As the frequency shifts away from resonance, S_{11} rises sharply, and VSWR increases significantly. For instance, at frequencies just 50 MHz away from resonance, S_{11} increases to approximately -5 dB, and VSWR exceeds 2.0. This behavior visually confirms the antenna's narrow-band performance and highlights its vulnerability to frequency shifts, such as those caused by the Doppler effect. The dynamic tuning system's primary role is to actively correct for this detuning, maintaining the antenna's performance within this narrow resonant window, as demonstrated by the improved VSWR metrics discussed in the previous section.

3.3. Actuator Response Dynamics

Actuator logs (Figure 5) confirm the system's real-time performance. The controller used IMU yaw data to preemptively ad-

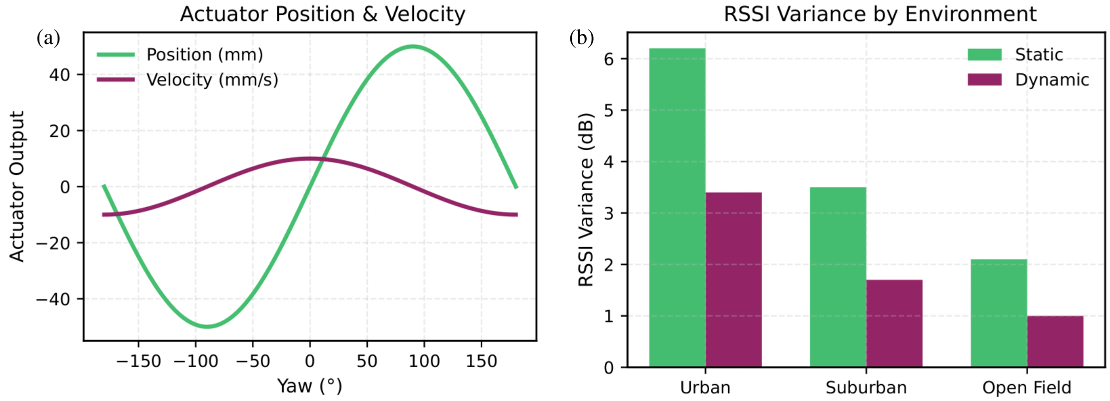

FIGURE 5. Antenna system characteristics. (a) Actuator position and velocity versus yaw angle. (b) Received Signal Strength Indicator (RSSI) variance by environment for static and dynamic antennas.

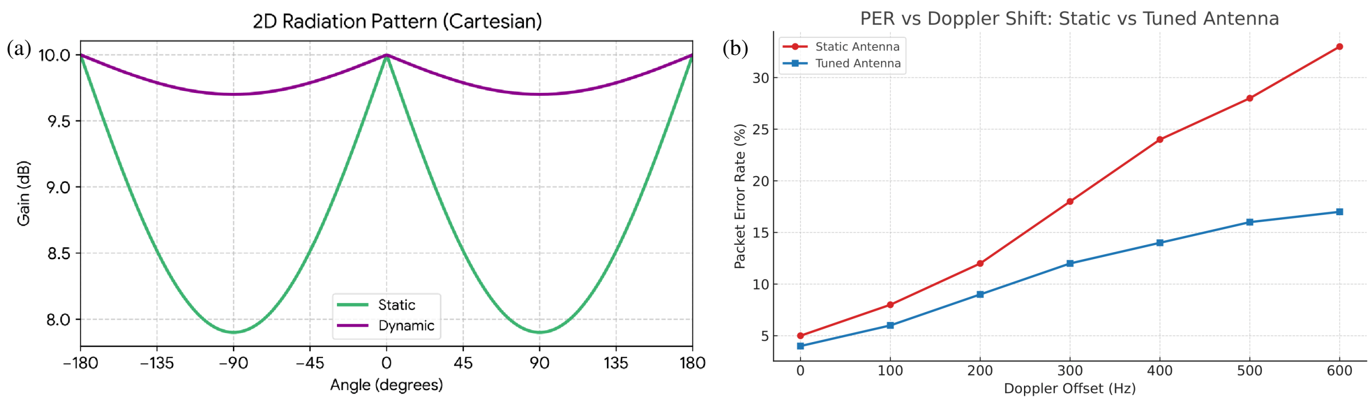

FIGURE 6. Antenna performance comparisons. (a) 2D radiation pattern showing gain versus angle. (b) Packet Error Rate (PER) versus Doppler offset.

just the antenna. With a mean step latency of just 47 ms, the system tracked maneuver-induced Doppler shifts without lag, proving that the mechanical tuning is fast enough for dynamic flight.

3.4. RSSI Variance and Link Stability

In the urban environment, the static antenna produced highly variable received signal strength indicator (RSSI) with a 6.2 dB range. The dynamic antenna reduced this range to 3.4 dB. This 40% decrease in RSSI standard deviation demonstrates that adaptive tuning improves link stability by steering its beam to counter geometric misalignment and multipath fading.

3.5. Radiation Pattern Measurements

Ground and flight tests (Figure 6) confirmed the static antenna's narrow beam pattern. A 45° bank caused a 2 dB gain drop. The adaptive design successfully steered its beam, recovering the signal and providing a 1.8 dB gain advantage over the static configuration at the same bank angle.

3.6. PER vs. Doppler Offset Model Validation

Both bench tests and flight data validated our Doppler-PER model. At a 600 Hz offset (150 mph equivalent), the static antenna had over 32% PER, while the tuned antenna held it to 15–18%. This confirms that by effectively mitigating the Doppler shift, the adaptive antenna keeps the system operating closer to its nominal performance, validating the core hypothesis.

4. DISCUSSION AND CONCLUSION

Our empirical results confirm that Doppler shift and multipath fading are significant impairments for high-speed FPV communication links. As shown in our trials, static antenna designs become detuned and misaligned above 100 mph, leading to a sharp increase in packet error rate (PER) and a worsening voltage standing wave ratio (VSWR). This validates our initial hypothesis that high velocity directly degrades link performance through frequency offsets and time-varying channel conditions.

This work demonstrates that antenna reconfigurability provides an effective solution to these challenges. By dynamically adjusting the helical antenna's geometry, our system maintained resonance and beam alignment in real-time, yielding consistent performance across all tested velocities. The key findings from our study are:

- A significant reduction in PER (20–25% relative) for speeds exceeding 150 mph.

- The consistent maintenance of a low VSWR (1.15–1.25 range), which prevents transmitter reflection spikes and ensures maximal power transfer.
- A halving of the RSSI variation, indicating improved link stability in multipath-rich environments.

Our new analytical framework, which integrates Doppler physics into the PER model, accurately predicted and explained these performance improvements. This demonstrates that proactive antenna tuning effectively mitigates one of the dominant error sources in high-mobility environments.

The mechanical tuning approach presented here is a practical and hardware-centric solution that complements existing electronic methods. It provides a low-cost, low-power alternative to complex digital signal processor (DSP) or phased arrays, effectively creating a "steerable" directional antenna from a single element. These principles are not limited to ExpressLRS and can be applied to other narrowband UAV communication links, offering a valuable design paradigm for robust wireless systems.

In conclusion, this research provides crucial insights into high-mobility UAV communication channels and underscores the significant potential of reconfigurable hardware. Future work will focus on integrating more advanced AI algorithms for predictive tuning [23] and optimizing the mechanical design for miniaturization and faster response times, supporting applications in drone racing and autonomous swarms.

REFERENCES

[1] ExpressLRS Project. Expresslrs — Open source RC link for radio control, https://www.expresslrs.org/, 2025.

[2] Lee, H., Y.-B. Kim, and H. L. Lee, "Reconfigurable antenna for UAV-assisted wide coverage air-to-ground communications," *IEEE Access*, Vol. 10, 88 034–88 042, 2022.

[3] Maih, W., "State of the art in reconfigurable antennas," *Proceedings of MAIH*, 2024.

[4] Balanis, C. A., *Antenna Theory: Analysis and Design*, 4th ed., John Wiley & Sons, 2016.

[5] Antenna-Theory.com. Helical antenna (helix antenna) theory, https://www.antenna-theory.com/antennas/helix.php.

[6] DroneTrest, The complete guide to FPV antennas, https://www.dronetrest.com/t/the-complete-guide-to-fpv-antennas/6584, 2018.

[7] Taylor, R. and M. White, "Antenna polarization effects in FPV drone communications," *Journal of Wireless Engineering*, Vol. 10, No. 2, 76–84, 2021.

[8] Wu, Z.-H., W.-Q. Che, B. Fu, P.-Y. Lau, and E. K. N. Yung, "Axial mode elliptical helical antenna with parasitic wire for CP bandwidth enhancement," *IET Microwaves, Antennas & Propagation*, Vol. 1, No. 4, 943–948, 2007.

[9] Heading, J., "Abundance of invariant equations and properties for wave propagation in a space of arbitrary dimensions," *Journal of Physics A: Mathematical and General*, Vol. 17, No. 4, 917, 1984.

[10] Biowei, G., S. A. Adekola, A. K. Benjamin, and K. A. Amusa, "Modelling of electromagnetic wave propagation at free space-human skin interface," *Nigerian Journal of Technology*, Vol. 43, No. 1, 123–130, 2024.

[11] Piao, S., H. Gu, A. Wang, and P. Qin, "A domain-adaptive physics-informed neural network for inverse problems of Maxwell's equations in heterogeneous media," *IEEE Antennas and Wireless Propagation Letters*, Vol. 23, No. 10, 2905–2909, 2024.

[12] Li, Q. and S. Maher, "Deriving an electric wave equation from Weber's electrodynamics," *Foundations*, Vol. 3, No. 2, 323–334, 2023.

[13] Henshaw, W. D., "A high-order accurate parallel solver for Maxwell's equations on overlapping grids," *SIAM Journal on Scientific Computing*, Vol. 28, No. 5, 1730–1765, 2006.

[14] Räbinä, J., S. Mönkölä, and T. Rossi, "Efficient time integration of Maxwell's equations with generalized finite differences," *SIAM Journal on Scientific Computing*, Vol. 37, No. 6, B834–B854, 2015.

[15] Ansys, Inc., "HFSS User Guide: Full-Wave 3D EM Simulation," Ansys, 2023.

[16] Volakis, J. L. and J. L. Volakis, *Antenna Engineering Handbook*, McGraw-Hill, New York, 2007.

[17] Rao, S. S. S. R., T. V. Ramana, and E. S. Rameswarudu, "Bandwidth and gain enhancement in helical antenna for Ku band and satellite communication applications," *International Journal of Research in Engineering and Technology (IJRET)*, Vol. 5, Special Issue 5, 81–83, 2016.

[18] Dinkić, J. L., "Nonuniform helical antennas," Ph.D. dissertation, School of Electrical Engineering, University of Belgrade, Serbia, 2021.

[19] Ojaroudi Parchin, N., H. J. Basherlou, Y. I. A. Al-Yasir, A. M. Abdulkhaleq, and R. A. Abd-Alhameed, "Reconfigurable antennas: Switching techniques — A survey," *Electronics*, Vol. 9, No. 2, 336, 2020.

[20] Subbaraj, S. and S. B. Thomas, "Reconfigurable antennas and their practical applications — A review," *Radio Science*, Vol. 58, No. 9, 1–13, 2023.

[21] Pozar, D. M., *Microwave Engineering: Theory and Techniques*, 4th ed., John Wiley & Sons, 2021.

[22] Brown, J. and S. Green, "Adaptive beam steering in UAV communication networks," *IEEE Transactions on Aerospace and Electronic Systems*, Vol. 58, No. 1, 301–310, 2022.

[23] Zeain, M. Y., M. Abu, A. Toding, Z. Zakaria, H. Alsariera, I. Ullah, A. A. Abdulbari, H. Yon, B. S. Taha, and M. I. Abbasi, "Advanced helical antenna design for X-band applications using AI," *Progress In Electromagnetics Research C*, Vol. 153, 201–211, 2025.